Modeling the Electrostatic Signature of Single Enzyme Activity

Landon Prisbrey, Guenter Schneider, and Ethan Minot*

Department of Physics, Oregon State University, Corvallis, Oregon 97330

Received: November 17, 2009; Revised Manuscript Received: February 3, 2010

Charge sensors based on nanoscale field-effect transistors are a promising new tool to probe the dynamics of individual enzymes. However, it is currently unknown whether the electrostatic signals associated with biological activity exceed detection limits. We report calculations of electrostatic signatures of two representative enzymes, deoxyribonuclease I and T4 lysozyme. Our simulations reveal that substrate binding to deoxyribonuclease and internal dynamics of lysozyme are detectable at the single-molecule level using existing point-functionalized carbon nanotube sensors.

Introduction

Enzyme function is closely linked to enzyme dynamics, and several techniques have been developed to probe this relationship. Nuclear magnetic resonance provides dynamic structural information but is an ensemble technique that cannot resolve the time sequence of events. Molecular dynamics simulations and single molecule fluorescence techniques[1] can elucidate the sequential nature of structural changes; however, the accessible time scales are limited. Molecular dynamics simulations running on supercomputers are still far from describing the whole turnover period of an enzyme (~1 ms), whereas single molecule fluorescence techniques are typically limited to time scales above 1 ms and less than a few seconds.

Nanoscale field effect transistors (nanoFETs) offer a new and complementary approach to track single-molecule activity by monitoring electrostatic fluctuations over a wide range of time scales. Electronic detection of a single molecule reaction was recently demonstrated by continuous, multihour monitoring of a charge-sensitive, nanoscale field-effect transistor (nanoFET).[2] This achievement motivates our theoretical work exploring the use of nanoFET charge sensors as a new tool to study enzyme dynamics at the single-molecule level.

The conductance of a nanoFET device changes as a function of local electrostatic potential, allowing the proximity of charges to be monitored. In an early example of nanoFET biosensing, a carbon nanotube (CNT) FET was used to measure the activity of a small ensemble of glucose oxidase enzymes.[3] More recent CNT-based experiments have used point functionalization to localize the detection volume of the nanoFET.[4] Such a device was used to monitor a single carboxylate group interacting with its immediate environment.[2] It has been proposed that these point-functionalized devices are ideally suited for sensing the activity of a single enzyme tethered to the point defect.[2] The simulations presented below focus on this proposed geometry (Figure 1).

The magnitude of electrostatic fluctuations generated by a single enzyme is a critical unknown in nanoFET schemes for sensing enzyme dynamics. The point-functionalized CNT devices currently used in experiments require a change in local electrostatic potential >10 mV to realize a conductance change that exceeds noise levels (within a 5 Hz−10 kHz bandwidth).[4] (We note that the 1/*f* dependence of the noise power spectral density in these sensors[4] allows for even faster sampling rates with little noise cost.) The electrostatics simulations presented in this work can be directly compared to this required minimum signal of 10 mV.

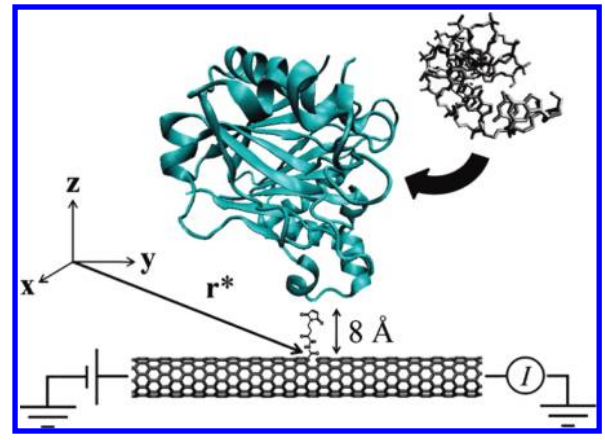

Figure 1. DNase I (ribbon representation, colored blue) conjugated to an activated carboxyl group on a CNT using *N*-[β-maleimidopropionic acid]hydrazide (BMPH). The conjugation point on DNase I is a mutated residue 240 (G240C). The conductance of the device changes upon binding of the DNA fragment (stick representation). The figure is drawn to scale.

NanoFET sensors offer functionality similar to single molecule fluorescence; therefore, it is instructive to consider the limitations of a typical single-molecule fluorescence experiment. The enzyme β-galactosidase is a model system for the detection of individual turnover events. Using confocal microscopy, it is possible to monitor these individual events for tens of seconds. Single turnover resolution is lost when the turnover rate exceeds 370 s^{-1} and the maximum turnover rate of 740 s^{-1} is inaccessible.[5] Our work suggests that the nanoFET approach will allow many enzymes to be studied at turnover rates that are orders of magnitude faster than this single-molecule fluorescence example.

To determine the electrostatic signature of single-molecule activity, we have exploited computational methods developed for modeling electrostatics in biological systems.[6−8] We solve the nonlinear Poisson−Boltzmann equation (NPBE) for multiple enzyme conformations along an enzymatic pathway for two enzymes. The first enzyme, deoxyribonuclease I (DNase I), is chosen to represent a class of enzymes in which the electrostatic signature of activity is expected to be dominated by the binding

* Corresponding author. E-mail: minote@science.oregonstate.edu.

10.1021/jp910946v

and unbinding of a charged substrate molecule. The second enzyme, T4 lysozyme (T4L), is chosen to represent a class of enzymes in which internal motion of charged protein regions is expected to dominate the electrostatic signature.

Methods

Figure 1 illustrates the geometry we have assumed for the nanoFET detection system. The enzyme is tethered site-specifically to the CNT defect using an 8-Å-long heterofunctional linker molecule (*N*-[β-maleimidopropionic acid]hydrazide) specifically designed to tether a cysteine residue to a carboxyl group. The coordinate **r*** denotes the position of the carboxyl defect. High-resolution crystal structures for DNase I[9] and T4L[10,11] were obtained from the Protein Data Bank, and charges were assigned to each atom of the enzyme using PDB2PQR[6,7] software employing the PARSE force field and using PROPKA to assign charges based on pK_a values and pH. Extraneous atoms (solvent, extra copies of the molecules, etc.) were deleted from the unit cell to leave only the molecules of interest. Three-dimensional maps of the electrostatic potential $\Phi(\mathbf{r})$ were generated by solving the NPBE with a standard finite element technique using the Adaptive Poisson−Boltzmann Solver (APBS) software[8] on a desktop computer. All software is freely available. In all calculations, a single ion for each ion boundary condition was used for an initial 150 × 150 × 150 Å box. This potential map was then used to set the Dirichlet boundary conditions for a smaller 75 × 75 × 75 Å box. The grid points of this final map were spaced 0.4 Å apart. Ion radius was 2 Å. The relative dielectric constants were set to 78.5 for the water and 1.0 for the interior of the protein. Alternative values of the protein dielectric constant have been tested, as discussed below. The concentration of monovalent ions was varied from 1 to 150 mM to examine screening effects. Divalent ions were not considered in any of our calculations, since the concentrations of Mg^{2+} and Ca^{2+} necessary for DNase and T4L activity (<100 μM) are well below the concentration of monovalent ions.

Results and Discussion

We first examine the electrostatic signature expected from enzymatic activity of DNase I (Figure 1). The DNase I enzyme cleaves the backbone of double-stranded DNA. The DNA backbone is highly charged, so the substrate binding event is a promising candidate for charge-sensitive detection. For our calculations, we used a 2.0 Å crystal structure of wild type DNase I bound to a short DNA fragment (bare charge, $-12e$).[9] Charges were assigned to the enzyme at pH 7.5. Each phosphate group in the DNA fragment's backbone was assigned a charge of $-1e$, and the remaining atoms were left uncharged. It is well-known that counterion condensation reduces the bare charge of DNA.[12] The effect of counterion condensation is adequately described by the NPBE calculation of APBS.[13,14]

Our goal is to calculate changes in the electrostatic potential at the carboxyl defect, $\Delta\Phi(\mathbf{r}^*)$, when the DNA substrate binds to the enzyme. Two electrostatic potential volume maps were generated: the first describes the field around the ligand-free enzyme, and the second describes the field around the DNA−enzyme complex. The CNT and linker molecule were not included in the calculation (see discussion below). Residue 240 (GLY) was chosen as the site-specific immobilization point on the enzyme. It is an exposed residue near the active site and could conceivably be mutated into a cysteine without significantly altering the enzyme's structure (glycine and cysteine are similar in size, and both are nonpolar and uncharged). The coordinate **r*** is set 8 Å from the α-carbon of residue 240 (8 Å is the length of the linker molecule) at a maximal distance from the protein surface. The distance between the bound DNA fragment and **r*** is ~40 Å. At 1 mM monovalent ion concentration, we calculate $\Phi(\mathbf{r}^*) = -22$ mV for ligand-free DNase and $\Phi(\mathbf{r}^*) = -47$ mV for complexed DNase. The calculated change in potential associated with binding the negatively charged substrate $\Delta\Phi(\mathbf{r}^*)$ is therefore −25 mV.

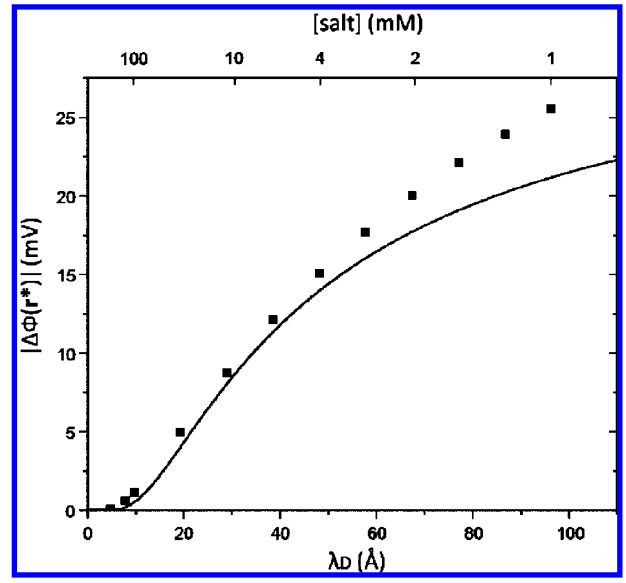

Figure 2. The electrostatic signal, $\Delta\Phi(\mathbf{r}^*)$, when the DNA fragment binds to DNase I. The solid line shows the approximation $\Delta\Phi_{\text{Coulomb}}(\mathbf{r}^*)$ given by eq 1.

The electrolyte concentration affects the ionic screening length and therefore affects $\Delta\Phi(\mathbf{r}^*)$. Following the procedures described above, we have calculated $\Delta\Phi(\mathbf{r}^*)$ over a range of salt concentrations. Figure 2 shows $\Delta\Phi(\mathbf{r}^*)$ (square data points) plotted as a function of Debye screening length,

$$\lambda_D = 9.62\ \text{Å}\sqrt{\frac{100\ \text{mM}}{[\text{salt}]}}$$

The magnitude of $\Delta\Phi(\mathbf{r}^*)$ exceeds the 10 mV noise threshold when $\lambda_D > 33$ Å ([salt] < 8 mM). We note that DNase I is highly active in this range of monovalent ion concentrations.

The calculated electrostatic signal at small λ_D is consistent with a screened Coloumb potential (Figure 2, solid line)

$$\Delta\Phi_{\text{Coulomb}}(\mathbf{r}^*) \cong \frac{1}{4\pi\varepsilon}\frac{q_{\text{DNA}}}{r}e^{-r/\lambda_D} \qquad (1)$$

where $r = 40$ Å and the DNA fragment's effective charge, q_{DNA}, is $-7e$. The effective charge was determined independently by accounting for counterion condensation on the DNA backbone. The solvent accessible surface area of each phosphate group was calculated. A buried group retains its bare charge of $-1e$, and a fully exposed group experiences a 75% reduction in charge due to counterion condensation.[15] Partially buried groups were assumed to retain a portion of their bare charge according to a linear relationship with exposed surface area. The deviations from $\Delta\Phi_{\text{Coulomb}}(\mathbf{r}^*)$ seen at lower salt concentrations (see Figure 2) are expected as counterion condensation becomes less significant.

The good agreement between the NPBE simulation and the Coulomb potential (eq 1) suggests that our simulation results

are insensitive to the dielectric constant of the protein. Indeed, we found that varying the relative dielectric constant of the protein between two extremes (1 to 20)[16] changed the calculated signal by only 13%.

We interpret $\Phi(\mathbf{r}^*)$ as representative of the average electrostatic potential felt at the carboxyl defect of the CNT sensor. This interpretation is based on the following assumptions: (i) The region of charge sensitivity around the point defect is small. This is consistent with scanning tunneling microscope spectroscopy studies that show the defect's electronic state does not extend more than 10 Å along the CNT axis.[17] (ii) The presence of the CNT and linker chain do not significantly perturb the potential at $\mathbf{r}^*$. This assumption is partially justified by the small volume occupied by the linker chain and the discrete nature of the CNT defect state. Theoretical investigations of the precise electronic structure and screening properties of the defect state are ongoing. (iii) Changes in $\Phi(\mathbf{r}^*)$ due to thermal motion of individual protein residues happen at very fast time scales ($\ll 0.1$ μs) and can be suppressed by time averaging. (iv) Translational and rotational motion of the entire enzyme due to center-of-mass thermal motion is fast (~ 0.1 μs),[18] and time averaging these fluctuations will lead to a measured potential $\Phi(\mathbf{r}^*)$ at the nanoFET sensor.

We have examined the final assumption in more detail to confirm that $\Phi(\mathbf{r}^*)$ is, indeed, representative of the potential after averaging over center-of-mass thermal motion. For ligand-free and DNA-bound DNase I in 1 mM ionic buffer, we calculated $\Phi(\mathbf{r})$ at 180 equally spaced solvent accessible points located 8 Å from residue 240 (the points cover a solid angle of 1.8π). The resulting distributions of potential are approximately Gaussian. The ligand-free form has a standard deviation of 17 mV and an average value of -21 mV, in close agreement with $\Phi(\mathbf{r}^*) = -22$ mV reported above. The DNA-bound form has a standard deviation of 18 mV and an average value of -50 mV, also in close agreement with the value reported above $\Phi(\mathbf{r}^*) = -47$ mV. The large standard deviations show that averaging over center-of-mass thermal motion time scales will be critical when looking for electrostatic signatures near the 10 mV minimum.

We now turn to a second enzyme in which an electrostatic signature of biological activity may be generated by intrinsic dynamics rather than binding of a charged substrate. T4 lysozyme is an extensively studied enzyme known to exhibit a dramatic conformational change upon cleaving bacterial cell walls.[19,20] The T4L structure consists of two charged regions with net charges $+3e$ and $+7e$. These regions move relative to each other in a hingelike motion (Figure 3). Single-molecule FRET studies suggest that this motion occurs on a millisecond time scale both with and without substrate present.[19] T4L maintains high activity over a broad range of electrolyte concentrations ([salt] < 100 mM).[21] In our calculations, the closed state was represented by a 1.7 Å crystal structure of wild type T4L.[10] For the open state, a 2.0 Å crystal structure of the I3P mutant was used.[11] This mutant has been shown to be representative of the open state of wild type T4L along its enzymatic trajectory.[20] Residues 163 (ASN) and 164 (LEU) were removed from open T4L so that the two structures would contain exactly the same residues. Charges were assigned to each atom at pH 7.2. Because the I3P mutant has a different residue at position 3, residue 3 was neutralized in both structures.

A natural choice for a conjugation site in T4L is residue 97, an exposed cysteine with a 22 Å^2 molecular accessible surface area. Residue 97 is on the $+7e$ region of T4L; therefore, for our simulations, we align the $+7e$ regions of open and closed

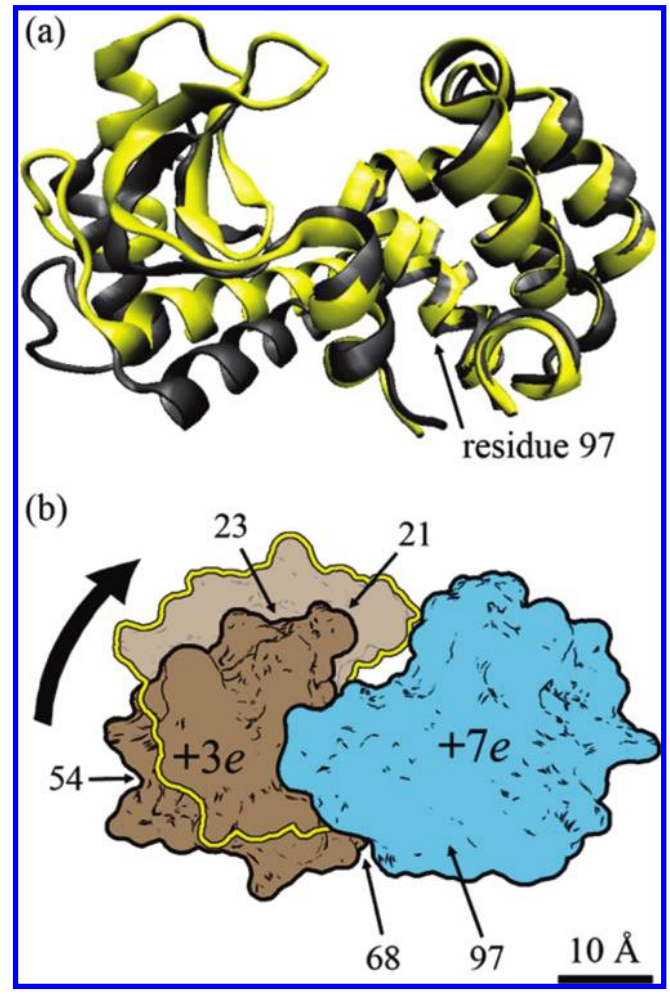

Figure 3. (a) The open (gray) and closed (yellow) structures of T4 lysozyme used in our calculations (Protein Data Bank identification codes 4LZM and 1L97, respectively). The two structures were aligned using the protein backbone around residue 97 (α-carbons of residues 93−101). In this alignment, the $+7e$ regions lie on top of each other, and the $+3e$ region moves about the hinge point. (b) Cartoon illustrating the position of the $+3e$ region relative to the $+7e$ region of T4 lysozyme. In the open configuration, the $+3e$ region is dark tan. In the closed-configuration the $+3e$ region is outlined in yellow. Arrows point to residues 21, 23, 54, 68, and 97, which were considered as possible site-specific attachment points.

TABLE 1: The Electrostatic Potential at the CNT Defect Site $\Phi(\mathbf{r}^*)$ for Each T4L Structure with 1 mM Monovalent Ion Concentration

$\Phi(\mathbf{r}^*)$ (mV)	full calculation	control calculation ($+7e$ region neutralized)
open	61	−13
closed	74	−1
difference	13	12

T4L (the near-perfect alignment is shown in Figure 3a). $\Phi(\mathbf{r})$ was calculated at $\mathbf{r}^*$, a point 8 Å away from the sulfur atom of residue 97, which maximized the distance between $\mathbf{r}^*$ and the protein surface. As a control experiment, we also calculated $\Phi(\mathbf{r}^*)$ when all charged residues in the $+7e$ region are neutralized. The results for 1 mM ionic buffer are show in Table 1.

Figure 4 shows the effect of varying λ_D on $\Delta\Phi(\mathbf{r}^*)$. It can be seen that the calculated change in potential between open and closed T4L exceeds the 10 mV noise limit for $\lambda_D > 13$ Å ([salt] < 55 mM). The control calculation (Table 1) shows that this signal can be attributed to large-scale motion of the $+3e$

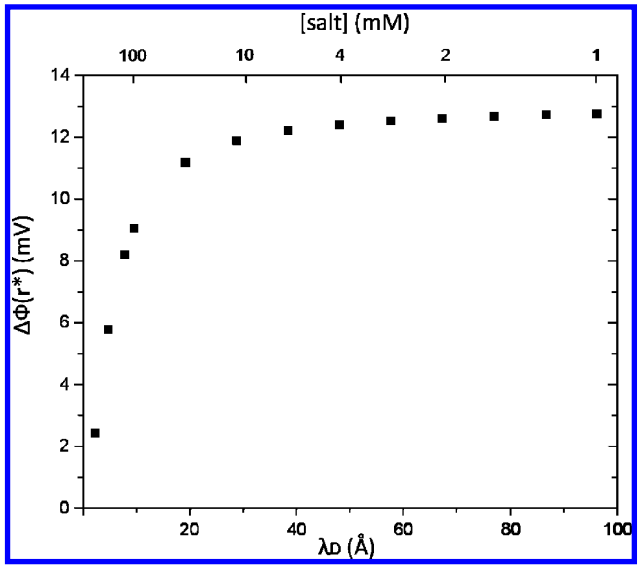

Figure 4. Effect of salt concentration on $\Delta\Phi(\mathbf{r}^*)$ for the intrinsic motion of T4 lysozyme.

region, rather than small-scale redistribution of atoms within the $+7e$ region.

Modeling the T4L system with a simple Coulomb potential (eq 1) is inadequate for predicting $\Delta\Phi(\mathbf{r}^*)$. The signal from T4L activity originates from movement of a complicated spatial distribution of charge, in contrast to the DNase/DNA system in which the DNA fragment can be approximated as a localized charge. The charge distribution associated with T4L must be described in detail to make a reasonable estimate of $\Delta\Phi(\mathbf{r}^*)$.

As was done with the DNase system, we calculated the fluctuations in $\Phi(\mathbf{r}^*)$ associated with center-of-mass thermal motion. For open and closed T4L in 1 mM ionic buffer, we calculated $\Phi(\mathbf{r})$ at approximately 60 equally spaced solvent-accessible points located 8 Å from residue 97 (these solvent-accessible points cover a solid angle of 0.7π). The resulting distributions are Gaussian-like and have means and standard deviations of 64 ± 11 mV for open T4L and 82 ± 15 mV for closed T4L. These average values agree with those reported in Table 1. The large standard deviations reinforce our conclusion that single-molecule sensing in the proposed nanoFET geometry will be limited to time scales slower than center-of-mass thermal motion time scales.

Even without optimizing the residue choice for site-specific immobilization, our calculations show that the hinge motion dynamics of T4L is potentially detectable with a nanoFET sensor. In an attempt to optimize signal strength, simulations were preformed for four different conjugation sites on the $+3e$ region. At a monovalent ion concentration of 1 mM, the calculated signal strengths were 10 mV (residue 21), 11 mV (residue 23), 0.4 mV (residue 54), and 5 mV (residue 68). Conveniently, the naturally occurring exposed cysteine (residue 97) gives the largest signal.

Conclusions

Our calculations show that the processes of substrate binding to DNase I and internal dynamics of T4L could be detected with a point-functionalized CNT sensor. At physiological salt concentrations ([salt] ~100 mM), signals are below the limits of detection for existing devices; therefore, we conclude that the general applicability of these sensors is currently limited to (i) studying enzymes that are active when salt concentrations are lower than physiological conditions (DNase I and T4L are both active at appropriately low salt concentrations) and (ii) studying enzyme processes involving highly charged substrate molecules. Although our modeling shows that the time resolution of single-molecule nanoFET sensing will not exceed the time scales of center-of-mass thermal motion, the predicted time resolution (~1 μs) is significantly faster than existing single-molecule techniques. We expect that application of our computational methods to more enzyme systems will reveal many biologically relevant single-molecule processes that are potentially detectable with nanoFET detection schemes. Additional applications of these computational methods will include the prediction of signals from nanoFET-based immunoassay sensors.[22]

Acknowledgment. We thank Leo Fifield, Michael Chapman, and Andy Karplus for useful discussions. This work was funded by the Office of Naval Research via the ONAMI Nanometrology and Nanoelectronics Initiative.

References and Notes

(1) Blank, K.; De Cremer, G.; Hofkens, J. *Biotechnol. J.* **2009**, *4*, 465–479.
(2) Goldsmith, B. R.; Coroneus, J. G.; Kane, A. A.; Weiss, G. A.; Collins, P. G. *Nano Lett.* **2008**, *8*, 189–194.
(3) Besteman, K.; Lee, J.; Wiertz, F. G. M.; Heering, H. A.; Dekker, C. *Nano Lett.* **2003**, *3*, 727–730.
(4) Goldsmith, B. R.; Coroneus, J. G.; Khalap, V. R.; Kane, A. A.; Weiss, G. A.; Collins, P. G. *Science* **2007**, *315*, 77–81.
(5) English, B. P.; Min, W.; van Oijen, A. M.; Lee, K. T.; Luo, G.; Sun, H.; Cherayil, B. J.; Kou, S. C.; Xie, X. S. *Nat. Chem. Biol.* **2006**, *2*, 87–94.
(6) Dolinsky, T. J.; Czodrowski, P.; Li, H.; Nielsen, J. E.; Jensen, J. H.; Klebe, G.; Baker, N. A. *Nucleic Acids Res.* **2007**, *35*, W522–525.
(7) Dolinsky, T. J.; Nielsen, J. E.; McCammon, J. A.; Baker, N. A. *Nucleic Acids Res.* **2004**, *32*, W665–667.
(8) Baker, N. A.; Sept, D.; Joseph, S.; Holst, M. J.; McCammon, J. A. *Proc. Natl. Acad. Sci. U.S.A.* **2001**, *98*, 10037–10041.
(9) Lahm, A.; Suck, D. *J. Mol. Biol.* **1991**, *222*, 645–667.
(10) Bell, J. A.; Wilson, K. P.; Zhang, X.-J.; Faber, H. R.; Nicholson, H.; Matthews, B. W. *Proteins: Struct., Funct., Genet.* **1991**, *10*, 10–21.
(11) Dixon, M. M.; Nicholson, H.; Shewchuk, L.; Baase, W. A.; Matthews, B. W. *J. Mol. Biol.* **1992**, *227*, 917–933.
(12) Manning, G. S. *Q. Rev. Biophys.* **1978**, *11*, 179–246.
(13) Das, R.; Mills, T. T.; Kwok, L. W.; Maskel, G. S.; Millett, I. S.; Doniach, S.; Finkelstein, K. D.; Herschlag, D.; Pollack, L. *Phys. Rev. Lett.* **2003**, *90*, 188103.
(14) Ballauff, M.; Jusufi, A. *Colloid Polym. Sci.* **2006**, *284*, 1303–1311.
(15) Keyser, U. F.; Koeleman, B. N.; van Dorp, S.; Krapf, D.; Smeets, R. M. M.; Lemay, S. G.; Dekker, N. H.; Dekker, C. *Nat. Phys.* **2006**, *2*, 473–477.
(16) Warshel, A.; Sharma, P. K.; Kato, M.; Parson, W. W. *Biochim. Biophys. Acta* **2006**, *1764*, 1647–1676.
(17) Berthe, M.; Yoshida, S.; Ebine, Y.; Kanazawa, K.; Okada, A.; Taninaka, A.; Takeuchi, O.; Fukui, N.; Shinohara, H.; Suzuki, S.; Sumitomo, K.; Kobayashi, Y.; Grandidier, B.; Stievenard, D.; Shigekawa, H. *Nano Lett.* **2007**, *7*, 3623–3627.
(18) We estimate the correlation time τ for the center-of-mass thermal motion of a tethered protein as the time the protein takes to diffuse a distance $x \approx 3$ nm ($\pi \times$ tether length). The diffusion time is given by $\tau = x^2/D$ where D is the diffusion constant of a small protein in water ($D \approx 10^{-6}$ cm^2/s).
(19) Chen, Y.; Hu, D.; Vorpagel, E. R.; Lu, H. P. *J. Phys. Chem. B* **2003**, *107*, 7947–7956.
(20) Zhang, X.; Wozniak, J. A.; Matthews, B. W. *J. Mol. Biol.* **1995**, *250*, 527–552.
(21) Priyadarshini, S.; Kansal, V. K. *J. Dairy Res.* **2003**, *70*, 467–471.
(22) Allen, B. L.; Kichambare, P.; Star, A. *Adv. Mater.* **2007**, *19*, 1439–1451.

JP910946V